J Appl Electrochem (2014) 44:773–779
DOI 10.1007/s10800-014-0685-z

RESEARCH ARTICLE

Electrochemical and structural characterization of AZ63 alloy surface film in $MgSO_4$ solution

Lin Chen · Changguo Chen · Ningning Wang · Yuping Liu · Jimin Wang · Ling Deng · Qiaoling Yang

Received: 9 December 2013 / Accepted: 17 March 2014 / Published online: 8 April 2014

Abstract The formation and growth of surface film on AZ63 (Mg–6Al–3Zn) magnesium alloys were studied in 2 M $MgSO_4$ aqueous solution using electrochemical methods. Surface examinations were carried out using scanning electron microscopy, energy-dispersive X-ray spectroscopy, and microscopic Fourier transform infrared spectroscopy. Experimental results show that the corrosion current decreases with prolonged immersion time, the three stages of hydrogen evolution rate correspond with the growth processes of the surface film on AZ63 magnesium alloys, and charge transfer resistance increases with the accumulation of corrosion products. A layer of MgO with sulfate salt grains underneath seems smooth at first. However, a few surface micro-cracks caused by inner stress appear on the smooth base film after 5 h of immersion, followed by the aggregation of spherical grains and the formation of cracks after 12 h. It is suggested that sulfate salt, carbonate salt, and hydroxide of magnesium should be the main composition of the surface film.

Keywords AZ63 · Magnesium alloy · Corrosion · Surface film

L. Chen · C. Chen (✉) · N. Wang · Y. Liu · J. Wang · L. Deng · Q. Yang
College of Chemistry and Chemical Engineering, Chongqing University, Chongqing 400044, People's Republic of China
e-mail: cgchen@cqu.edu.cn

L. Chen
College of Material and Chemical Engineering, Sichuan University of Science and Engineering, Zigong 643000, People's Republic of China

1 Introduction

Magnesium is a research priority in the energy field because of its advantages, including negative electrode potential, high theoretical capacity of up to 2.22 Ah g^{-1}, rich resource, and environmental friendliness [1–3]. Compared with the conventional Zn–MnO_2 dry cell, the Mg–MnO_2 dry cell demonstrates significantly better properties, such as 0.3–0.4 V higher average work voltage, two times higher capacity under large current discharge, over 80 % retention of the initial capacity after 2 years of storage, and absence of mercury and other toxic substances [4]. The negative electrode of the Mg battery is usually made of AZ series alloys. Although the AZ31 alloy has relatively higher discharge efficiency, it has a voltage delay problem. Meanwhile, the AZ21 alloy is commonly used because it can improve current efficiency and reduce voltage delay. Voltage delay is a complex electrochemical dynamic process that is associated with the corrosion of Mg electrode in electrolyte. During discharging, the voltage delay of Mg batteries is due to the formation of passive film on the negative electrode's surface. Knowledge on the formation, growth, and structure of the film would help elucidate corrosion dynamics. However, related research work remains insufficient and incomplete to date. Therefore, further studies are necessary.

When exposed to dry and clean air, the fresh surface of pure Mg immediately forms a hydrated layer of gray film. The film has an amorphous structure composed of Mg, MgO, and 50–60 % $Mg(OH)_2$ [5]. X-ray photoelectron spectroscopy (XPS) was carried out to analyze the film and observe H_2O molecular and dissociative (OH) water adsorption [6]. A reaction mechanism was postulated in which the topmost layer of MgO is converted to $Mg(OH)_2$ upon dissociation of water, and the oxide portion of the

MgO film becomes thinner upon hydroxylation. The initial film formed on the Mg mechanically treated surface upon immersion in aqueous electrolyte has a bilayer structure consisting of an inner MgO layer and an outer $Mg(OH)_2$ layer [7]. The second phase enrichment phenomenon occurs when Mg alloys containing Al, Mn, and Zn are isolated in the atmosphere. The level structures of the MgO film in vapor contain MgO/Mg–Al–O/substrate metal layers, and the oxides with rich Mg become thinner as the content of Al increases [8–10]. In dilute NaCl solutions, the surface film formed on AZ31 Mg alloy surface is polarized in both zones. XPS results indicate the presence of MgO, $Mg(OH)_2$, and $MgCO_3$ on the surface film [11].

Song et al. [12] indicated that the surface film of AZ21 in NaCl solution may consist of three layers without clear interphases: $Mg(OH)_2/MgO/Al_2O_3/Mg$. The surface film on AZ501 presents a model of $(Al, Mg)_n(OH)_m/(Mg,Al)_yO_x/Mg$. The surface film on the AZ91 alloy with both α and β phases is expected to be similar to the combination of those on AZ21 and AZ501. They found that AZ91 alloys with β phase have relatively lower corrosion rate and better passivation. Corrosion products for ingots are mainly $Mg(OH)_2$ with small amounts of β phase, $Mg–Al_2O_3$, and MgH_2, whereas those for die-cast show a highly amorphous structure [13–15]. Generally, the anticorrosion performance of most Mg alloys in neutral solution is not good. The reason might be the corrosion products formed are farther from the anode surface, are very loose, and are easy to flake away as $Mg(OH)_2$ tends to deliquesce [16]. Studies [17–20] show that Mg alloy surface in humid environment or in most solutions is mostly covered with a layer of oxide film that consists of insoluble Mg salts, such as MgO, $MgCO_3$, and $Mg(OH)_2$.

A layer of corrosion film can easily form on the surface of AZ63 Mg alloy. Information on the properties of the corrosion film would facilitate understanding of the voltage delay of Mg primary batteries. In this paper, the formation and growth of surface films on Mg alloy are illustrated. The electrochemical performance, components, and micromorphology of the film at various stages were also investigated. The results of this study will provide basic theoretical data to understand the voltage delay of Mg primary batteries.

2 Experimental

AZ63 Mg alloy was provided by Ao-Xin Anticorrosion Materials Co., Ltd. (Jiaozuo, China). The chemical composition of the alloy was (wt%) 5.52 % Al, 2.94 % Zn, 0.218 % Mn, 0.180 % Si, 0.109 % S, and balance Mg. The specimens were 10 mm × 10 mm × 5 mm in size and were grounded with 400 #, 600 #, 800 #, and 1000 # grit SiC paper. Subsequently, the samples were cleaned in an ultrasonic bath in distilled water and acetone, and then dried in warm air. The specimens were linked by electrical wire and embedded in epoxy resin, and they were used as the working electrodes for the electrochemical measurements. The exposed surface area was $\sim 1\ cm^2$.

In this study, the hydrogen evolution rate from the samples was measured for 12 h in 2 M $MgSO_4$ solution, and the hydrogen evolution rate was calculated in $mL\ cm^{-2}\ h^{-1}$. The corrosion rate of Mg alloys exposed to aqueous solution was measured by recording the volume of hydrogen gas that evolved. The volume of hydrogen evolved was obtained by capability measurements that is, specimens were placed in a 500 mL beaker, which was a bottom-up filler attached with a burette. Before the test, the beaker and burette were filled with $MgSO_4$ solution. The volume of hydrogen that evolved was obtained using the scale of the burette [21]. Approximately 400 mL of naturally aerated 2 M $MgSO_4$ solution at 20 ± 2 °C was used as the electrolyte. The pH of the electrolyte was ~8.0 at the beginning of each experiment. All chemicals in this work were of analytical grade. The specimens were constantly immersed in $MgSO_4$ solution from 0.33 to 12 h.

Electrochemical experiments were carried out in a corrosion cell containing 400 mL of electrolyte using a standard three-electrode configuration with saturated calomel as the reference electrode and a graphite club as the counter electrode. All experiments were conducted at room temperature without stirring. Open circuit potential test results, polarization curve and electrochemical impedance spectroscopy (EIS) results were recorded using CH Instruments electrochemical measurement system (CHI660A, USA). The polarizations started from −1.8 V, and the scanning rate was 0.5 $mV\ s^{-1}$. EIS results were obtained at open circuit potentials in the frequency range of 10^5–10^{-2} Hz, with a sinusoidal signal perturbation of 10 mV. The experimental data were fitted with Zview2 software, and the errors were lower than 5 %.

Film thickness was measured by an eddy current thickness meter (DKD-K-33101, Germany), with a range of 0 ± 2,000 μm and the measured error ±0.5 μm, and five points on Mg surface were tested to ensure the data correct. The surface morphologies of the samples were observed by a SEM (VEGA 3, Czech Republic) coupled with energy-dispersive X-ray spectrometer at a working voltage of 20 kV. Fourier transform infrared spectroscopy (FT-IR) analyses were carried out using a NicoletiZ10 microscopic FT-IR spectrometer, and scan signals were the average of 50 readings. All electrochemical and analytical experiments were repeated until the results were consistent.

3 Results and discussion

3.1 Corrosion current change and hydrogen evolution rate

Figure 1 shows a comparison of the polarization curves for the alloys with different immersion time. After immersion, most of the curves exhibit a similar shape with a plateau extending on the anodic potential domain. Generally, the cathodic polarization curves mainly represent the cathodic hydrogen evolution. By Tafel plot, the corrosion current density (I_{corr}) can be readily calculated from Fig. 1.

Figure 2 presents the corrosion current density of AZ63 Mg alloys fluctuating with immersion time. The interaction effects of immersion time and pH on film thickness are presented in Table 1. As shown in Table 1, the open circuit potential value (E_{ocp}) and corrosion potential (E_{corr}) increase with prolonged immersion time. This result indicates the gradual increase in thermodynamic stability and corrosion resistance of the surface films. The corrosion current shifts decreased with prolonged immersion time because the corrosion film grows on the surface of the AZ63 Mg alloy. The I_{corr} values rapidly decrease before the immersion time reaches 3 h, indicating that the reaction rate is very fast during this period. At the same time, shown in Table 1, the growth rate of the surface film is fast. The lower corrosion current after 5 h of immersion indicates slow reaction rate, which suggests that the volume of evolved hydrogen decreases and that the growth rate of the alloy surface film becomes slow. The current density after 1 h of immersion is two times more than the current density after 5 h of immersion. This result reveals that the surface film can prevent the anodic process effectively and can stabilize the solid dissolution.

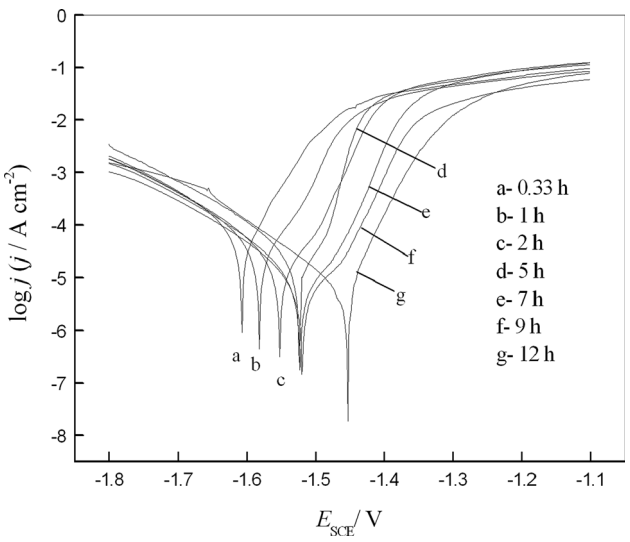

Fig. 1 Polarization curves for AZ63 Mg alloys in naturally aerated 2 M $MgSO_4$ solution and their dependence on immersion time. Potential sweep rate is 0.5 mV s^{-1}

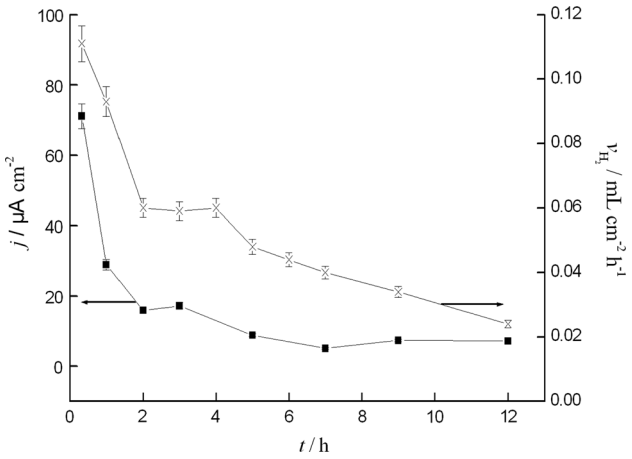

Fig. 2 Variation of corrosion current and hydrogen evolution rate of AZ63 Mg alloys with immersion times in 2 M $MgSO_4$ solution

As shown in Fig. 2, the hydrogen volume vs. time curve consists of three stages: from 0.33 to 2 h, the corrosion rate decreases very fast; from 2 to 4 h, the corrosion rate is steady and the hydrogen evolution rate remains at 0.06 mL cm^{-2} h^{-1}; and after 5 h, the hydrogen evolution rate decreases linearly with immersion time based on Eq. (1), where v_{H2} (mL cm^{-2} h^{-1}) is hydrogen evolution rate, t (h) is immersion time and R is the correlation coefficient. Hydrogen evolution rate measurements of the alloys show that the growth of the surface film is the main reason for the decrease in the corrosion rate.

$$v_{H2} = -0.00338\,t + 0.0643\,(R = 0.999) \quad (1)$$

The thickness of film follows the parabolic law based on Eq. (2), where d (μm) is film thickness, t (h) is immersion time, and R is correlation coefficient:

$$d = -0.0118\,t^2 + 0.256\,t + 0.713\,(R = 0.975) \quad (2)$$

Equation (2) reveals typical diffusion-controlled film growth and d is proportional to the square root of t, which is derived from the Fick's second law for diffusion process with semi-infinite boundary condition. The d–t curve after immersion of 5 h is close to a line, but the film thickness can not consist with the anode reaction rate. The film's growth rate depends not only on the anodic reaction rate, but also on the structure of the surface of magnesium alloys.

The initial pH of 2 M $MgSO_4$ solution is 8.04, which increases to 8.34 after 2 h of immersion. This result shows that pH increases as the number of OH^- ions increases. Therefore, hydrogen evolution causes the accumulation of OH^- ions, leading to the formation of $Mg(OH)_2$ on the surface in the early stage of immersion. When these reaction processes continue, the formation of $Mg(OH)_2$ results

Table 1 Variation of potential, pH, and film thickness with different immersion times

Immersion time (h)	0.33	1	2	5	7	9	12
E_{ocp} (V)	−1.668	−1.672	−1.660	−1.662	−1.658	−1.660	−1.642
E_{corr} (V)	−1.596	−1.554	−1.519	−1.489	−1.480	−1.480	−1.464
pH	8.08	8.09	8.34	8.49	8.42	8.46	8.43
Film thickness (μm)	0.6	1.1	1.3	1.7	1.8	2.1	2.1

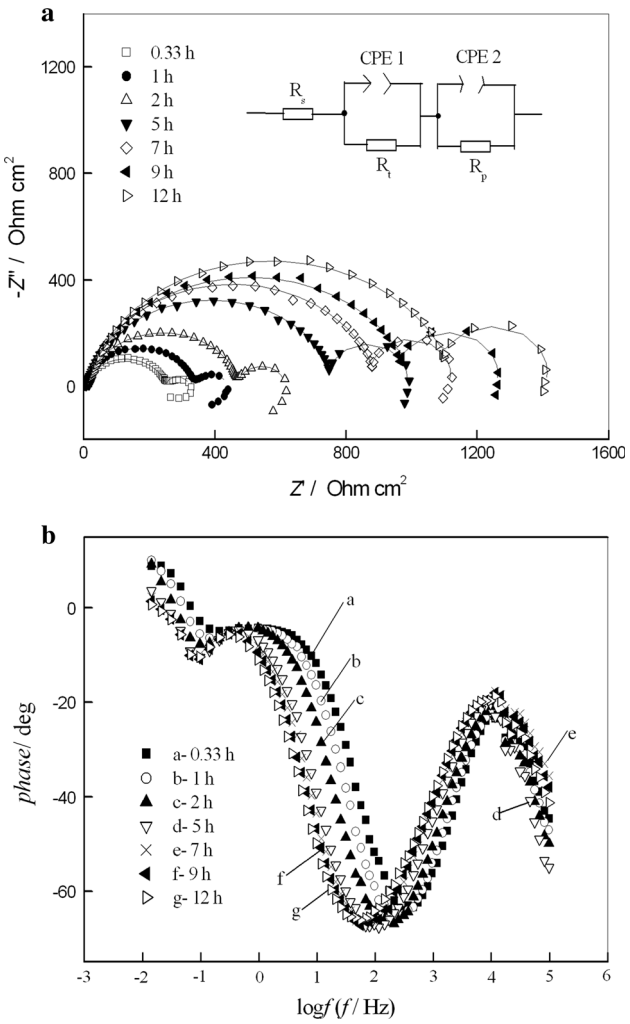

Fig. 3 Electrochemical impedance diagrams for surface film on AZ63 Mg alloys at E_{ocp} in 2 M $MgSO_4$ solution, and their dependence on immersion time. **a** Nyquist plot. Equivalent electrochemical circuit is presented in the insertion; **b** Bode plot. *Symbols* are experimental data and *lines* are fitted ones

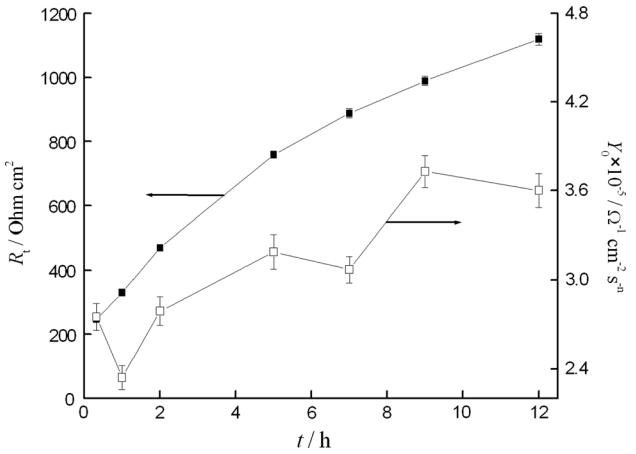

Fig. 4 The dependence of R_t and Y_0 values on immersion time in 2 M $MgSO_4$ solution. Exponent factors n from 0.33 to 12 h at higher frequency: 0.88, 0.91, 0.90, 0.90, 0.91, 0.88, and 0.89

in a dynamic balance of Mg^{2+} and OH^- ions, making the final pH remain almost constant.

3.2 Electrochemical impedance behavior

Electrochemical impedance diagrams for the surface film on AZ63 alloy obtained at open circuit potentials for different immersion times are shown in Fig. 3. The Nyquist and Bode plots of these impedance spectra, obtained by monitoring the film formation time, reveal two consecutive capacitive loops. The impedance spectra have the same characteristics, which indicates that the reaction process (or mechanism) involved in the film formation does not change with immersion time, but the properties of the surface film can change.

The electrochemical impedance spectra can be illustrated as [R_s(CPE1 R_t)(CPE2 R_p)] equivalent circuit (Fig. 3a), where R_s is the ohmic resistance of the cell, R_t is the charge transfer resistance, and CPE1 represents the electric double layer capacitance, R_p and CPE2 are the film resistance and constant phase angle element of the surface passive film on the anode, respectively. The CPE is defined by two values, Y_0 and n. If n is equal to 1, CPE is identical to a capacitor. The charge transfer resistance or film resistance is a measure for impediment to electron exchange reaction at the interface between metal and electrolyte, i.e., metal dissolution coupled with hydrogen evolution. The experimental data were fitted with Z-view software, and the main fitted parameters are shown in Fig. 4.

The first semicircle at higher frequency is related to R_t and CPE1. The semicircular diameter is defined by the charge transfer resistance and the electric double layer capacitance. R_t gradually increases as the immersion time is prolonged to 12 h. The experimental data fit well to an equivalent circuit consisting of R_t and CPE1 as a constant

phase element, as shown in Fig. 3. Corrosion resistance is characterized by the rate of charge transfer through the passive electrochemical interface, which experimentally reflects R_t value. And R_t value obtained from the data fitting increases by 132.4 Ω cm^2 as the immersion time is prolonged from 0.33 to 2 h but only by 60.2 Ω cm^2 from 5 to 9 h. This result indicates that the electrochemical reaction speed is significantly lower than that at the beginning as the film growth rate decreases significantly after 5 h of immersion.

The second semicircle at lower frequency may be caused by the deposition and dissolution of the corrosion products. Usually the semicircle at lower frequency indicates a diffusion process called "diffusion admittance." This phenomenon is caused by the change in capacitance on rough surface electrode, and its equivalent circuit can be represented by CPE. The value of R_p depends on the increase and densification of surface film thickness, which can affect the reaction rate. The reaction resistance of the adsorption product on the interface of Mg alloy/$MgSO_4$ changes significantly as the immersion time is prolonged. Moreover, the Nyquist plots show that diffusion is gradually weakened as the reaction time is prolonged, suggesting that the rotation angle between the semicircle's diameter and the real axis decreases. The exponent n of a CPE denotes the increase in real surface area on the Mg electrode resulting from the roughening of the surface film with prolonged immersion time. As the film grows, the exponent n of the CPE approaches 1 after 9 h of immersion, even though the roughness of the surface film seems to increase, which is mainly caused by the adsorption reduction of hydrogen on the metal/solution interface. In this case, the hydrogen evolution reaction makes the double layer significant thin with prolonged immersion time, and diffusion admittance decreases a little.

3.3 SEM analysis

After 0.33 h of immersion in the solution, the surface of the Mg alloy is covered with small smooth yellow flake-like product. A dark grayish layer studded with a few white grains appears on the alloy surface. These irregular grains are almost perpendicular to the surface and grow from the base film. Figure 5 shows the SEM images of the films immersed in $MgSO_4$ electrolyte for different times. The morphology after 1 h of immersion is shown in Fig. 5a. Several thin sea horse-like products begin to grow along with the phase interfaces and gradually connect. As shown in Fig. 5b, a few irregular grains studded underneath the base film can be observed. These grains detach from the base film and leave holes during the film formation's initial stage, suggesting that the grains originate from the base film. After 3 h of immersion, many grains protrude out of the film and aggregate to form sphere-like grains (Fig. 5c).

EDX spectroscopic data are meaning and valuable because the surface film on AZ63 alloy is entirely amorphous and the structural characterization of the film can not be obtained although the special methods, such as high-power (18 kW) X-ray diffraction, were used. As shown in Table 2, Mg and O atomic percent in zone A in Fig. 5c are 47.56 and 43.67. The consumed percent of O element can be calculated if the metal oxide is Al_2O_3 and ZnO in the base film, so Mg/O atomic ratio of Mg compound is larger than 1:1, and this result suggests that MgO should be the major component of the base film formed on the surface of AZ63 alloy in 2 M $MgSO_4$.

Although H cannot be detected by EDX, the components of the surface film can be estimated from Table 2. The content of S and C in zone B is 3.23 and 5.52 at.%, so 29.48 at.% O is estimated to be consumed because the groups of SO_4^{2-} and CO_3^{2-} are included in the surface film. The total content of O combining with Al, Zn, and Mn is about 6.40 at.%, which is calculated according to some usual oxides, then the remnant percent of O element that could combine with Mg element is 32.25 at.%. Considering the Mg atomic percent is 18.79, the Mg/O atomic ratio in zone B is approximately closed to 1:2, which suggests the presence of $Mg(OH)_2$. At the same time, due to $MgSO_4$ on the surface film has formed, consuming lots of Mg^{2+} ions coming from Mg corrosion and SO_4^{2-} ions in the electrolyte, therefore, magnesium sulfate salt ought to be the main component of the light-colored grains.

Several small micro-cracks appear on the smooth base layer after 5 h of immersion, which corresponds to the fact that the breadth increase in film ohmic resistance begins to decrease at the same time. As the immersion time is prolonged to 12 h, the surface film turns into snuff color. The number of grains increases, and numerous micro-cracks aggregate in the base film (Fig. 5d).

With prolonged immersion time, film densification blocks the H_2 release channels, causes H atom accumulation and creates high inner stress, ultimately leading to the formation of cracks and trenches in the film. The durative anode reaction processes result in a more compact and thicker base film, which decreases the hydrogen evolution rate after 12 h of immersion. Based on the analysis of the three stages of H_2 evolution rate in Fig. 2 and the SEM images in Fig. 5, the "metal dissolution–film expansion–film breakdown" model [22] is also likely to illustrate the surface film growth process on AZ63 Mg alloy in $MgSO_4$ solution.

3.4 Microscopic FT-IR spectra of the surface film

The reflection microscopic FT-IR spectroscopy was used to further identify the composition and structure of the surface film on AZ63 Mg alloy. Figure 6 shows the FT-IR spectra

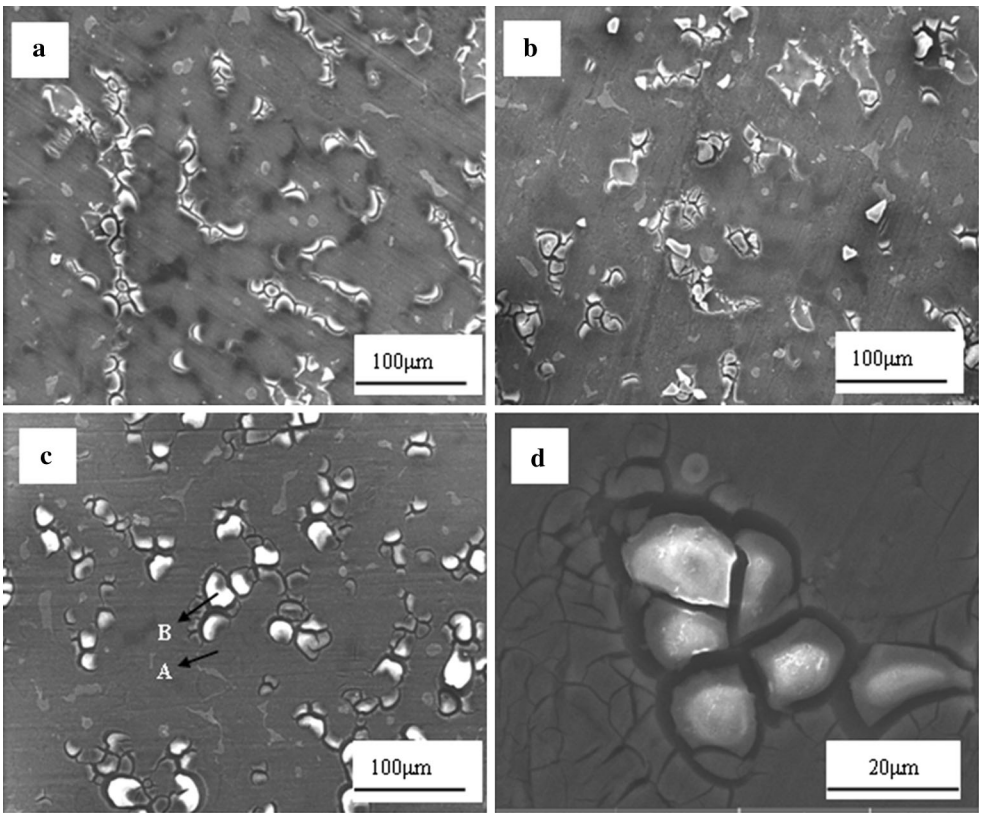

Fig. 5 SEM morphologies of films on AZ63 Mg alloys for 1 h (**a**), 2 h (**b**), 3 h (**c**) and 12 h (**d**) after immersed in 2 M $MgSO_4$ solution

Table 2 Element content of surface film of AZ63 Mg alloy in 2 M $MgSO_4$ solution (A-smooth surface; B-white grain)

Element content (at.%)	O	Mg	C	Al	Zn	S	Mn
A	43.67	47.56	–	5.09	1.47	2.21	–
B	68.13	18.79	5.52	2.18	1.13	3.23	1.00

of the surface film immersed in 2 M $MgSO_4$ solutions from 0.33 to 12 h. The peak height ratio at 3,450 and 1,630 cm^{-1}, accompanied by a stretching vibration (υ_{H2O}) and a bend vibration (δ_{H2O}), is considerably higher than that of adsorptive water, whose ratio is 1:0.3. The peak at 3,699 cm^{-1} is the characteristic peak of O–H stretching related to $Mg(OH)_2$ [23]. However, shown in Fig. 6, there is not any significant peak detected by FT-IR peak from 3,700 to 3,650 cm^{-1}, so the FT-IR spectroscopic results confirm that $Mg(OH)_2$ is amorphous in the conversion layer. And the strong absorption from 3,300 to 3,700 cm^{-1} is obviously induced by the stretching vibration of OH^-, therefore, amorphous $Mg(OH)_2$ should be supposed to be one of the components of the surface film.

The peak around 1,390 cm^{-1} in Fig. 6 could also be contributed to $\upsilon_3(CO_3^{2-})$, which indicates that a carbonate salt layer exists on the surface of AZ63 Mg alloy because

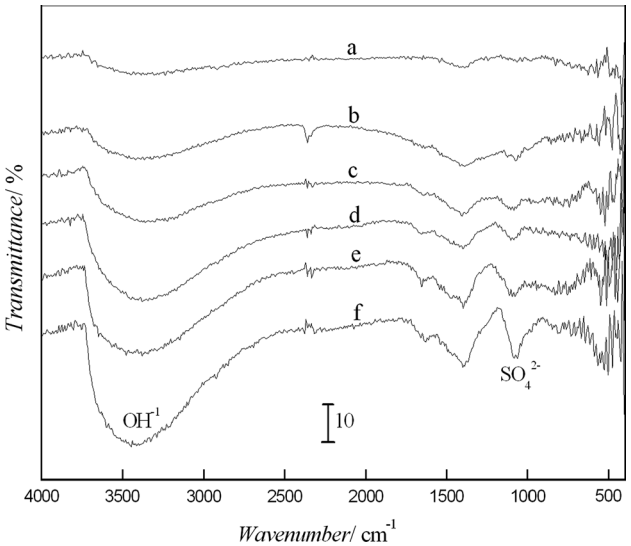

Fig. 6 Microscopic FT-IR spectra of surface film and dependence on immersion time. **a** 0.33 h, **b** 1 h, **c** 2 h, **d** 5 h, **e** 7 h, and **f** 12 h

of the chemical reaction. The SO_4^{2-} ion belongs to the five-atom tetrahedron group, and the characteristic frequency of SO_4^{2-} in the FT-IR spectra is generally at υ_3 (strong absorption at 1,210–1,040 cm^{-1}) and υ_4 (at

670–600 cm^{-1}). The strong peak at 1,080 cm^{-1} should be the frequency of $\upsilon_3(SO_4^{2-})$.

Hence, it is concluded that sulfate salt, carbonate salt, and hydroxide of magnesium should be the main composition of the surface film.

4 Conclusions

1 As the immersion time in 2 M $MgSO_4$ is prolonged, the surface film on AZ63 Mg alloys becomes thicker and rougher, I_{corr} decreases with prolonged immersion time, the hydrogen evolution rate gradually decreases, the constant phase element and the charge transfer resistance increase.

2 The structure of the surface film on the AZ63 Mg alloy in $MgSO_4$ solution shows that a MgO base layer is studded with irregular grains, which aggregate to form spherical grains with a diameter of ~ 10 μm.

3 The growth process of the film corresponds with the three stages of H_2 evolution rate. As the reaction time gradually approaches 12 h, inner stress accumulates, and numerous micro-cracks appear on the smooth base film.

4 The corrosion film on the AZ63 Mg alloys surface primarily consists of sulfate compound and hydroxide.

Acknowledgements Financial supports by the National Natural Science Foundation of China (No 21273292) and the Project of Material Corrosion and Protection Key Laboratory of Sichuan Province (2010CL01) are gratefully acknowledged.

References

1. Vuorilehto K (2003) An environmentally friendly water- activated manganese dioxide battery. J Appl Electrochem 33:15–21
2. Sivashanmuga A, Kumar TP, Renganathan NG, Gopukumar S (2004) Performance of a magnesium–lithium alloy as an anode for magnesium batteries. J Appl Electrochem 34:1135–1139
3. Zhao QS, NuLi YN, Guo YS, Yang J, Wang JL (2011) Reversibility of electrochemical magnesium deposition from tetrahydrofuran containing pyrrolidinyl magnesium halide solutions. Electrochim Acta 56:6530–6535
4. Jugović B, Gvozdenović M, Stevanović J, Trišović T, Grgur B (2009) Corrosion behavior of magnesium, aluminum and zinc as anodic materials in chloride based electrolytes for use in primary and secondary electrochemical power sources. Mater Des 30: 3291–3294
5. Nordlien JH, Ono S, Masuko N, Nisancioqlu K (1997) A TEM investigation of naturally formed oxide films on pure magnesium. Corros Sci 39:1397–1414
6. John TN, David ES, Susumu Y, Sarp K, Tom K, Erin RM, Soeren P, Miquel BS, Gordon EBJ, Anders N, Hendrik B (2011) Formation of hydroxyl and water layers on MgO films studied with ambient pressure XPS. Surf Sci 605:89–94
7. Santamaria M, Quarto FD, Zanna S, Marcus P (2007) Initial surface film on magnesium metal: a characterization by X-ray photoelectron spectroscopy (XPS) and photocurrent spectroscopy (PCS). Electrochim Acta 53:1314–1324
8. Splinter SJ, Mclntyre NS, Lennard WN, Grifliths K, Palumbo G (1993) An AES and XPS study of the initial oxidation of polycrystalline magnesium with water-vapor at room- temperature. Surf Sci 292:130–144
9. Splinter SJ, Mclntyre NS (1994) The initial interaction of water-vapor with Mg-Al alloy surfaces at room- temperature. Surf Sci 314:157–171
10. Mcintyre NS, Chen C (1998) Role of impurities to Mg surfaces under ambient exposure conditions. Corros Sci 40:1697–1709
11. Wang L, Shinohara T, Zhang BP, Iwai H (2009) Characterization of surface products on AZ31 magnesium alloy in dilute NaCl solution. J Alloy Compd 485:747–752
12. Song GL, Atrens A, Wu XL, Zhang B (1998) Corrosion behaviour of AZ21, AZ501 and AZ91 in sodium chloride. Corros Sci 40:1769–1791
13. Ambat R, Aung NN, Zhou W (2000) Evaluation of microstructural effects on corrosion behaviour of AZ91D magnesium alloy. Corros Sci 42:1433–1455
14. Li Y, Zhang T, Wang FH (2006) Effect of microcrystallization on corrosion resistance of AZ91D alloy. Electrochim Acta 51: 2845–2850
15. Chen J, Wang JQ, Han EH, Dong JH, Ke W (2007) AC impedance spectroscopy study of the corrosion behavior of an AZ91 magnesium alloy in 0.1 mol L^{-1} sodium sulfate solution. Electrochim Acta 52:3299–3309
16. Singh Raman RK, Birbilis N, Efthimiadis J (2004) Corrosion of Mg alloy AZ91-the role of microstructure. Corros Eng Sci Technol 39:340–350
17. Eliezer D, Uzan P, Aghion E (2003) Effect of second phases on the corrosion behavior of magnesium alloys. Mater Sci Forum 419–422:857–866
18. Frankel GS, Samaniego A, Birbilis N (2013) Evolution of hydrogen at dissolving magnesium surfaces. Corros Sci 70: 104–111
19. Pérez P, Onofre E, Cabeza S, Llorente I, Del Valle JA, García-Alonso MC, Adeva P, Escudero ML (2013) Corrosion behaviour of Mg–Zn–Y Mischmetal alloys in phosphate buffer saline solution. Corros Sci 69:226–235
20. Vrátná J, Hadzima B, Bukovina M, Janeček M (2013) Room temperature corrosion properties of AZ31 magnesium alloy processed by extrusion and equal channel angular pressing. J Mater Sci 48:4510–4516
21. Aung NN, Zhou W (2010) Effect of grain size and twins on corrosion behaviour of AZ31B magnesium alloy. Corros Sci 52:589–594
22. Sathyanarayana S, Ratna Kumar BV (1983) The delayed action of magnesium anodes in primary batteries: Part II Theoretical studies. J Power Resour 10:243–261
23. Li YP, Tan CH, Qi GW, Guo J, Wang X, Zhang SY (2013) Decanoate conversion layer with improved corrosion protection for magnesium alloy. Corros Sci 70:229–234